ChemComm

Accepted Manuscript

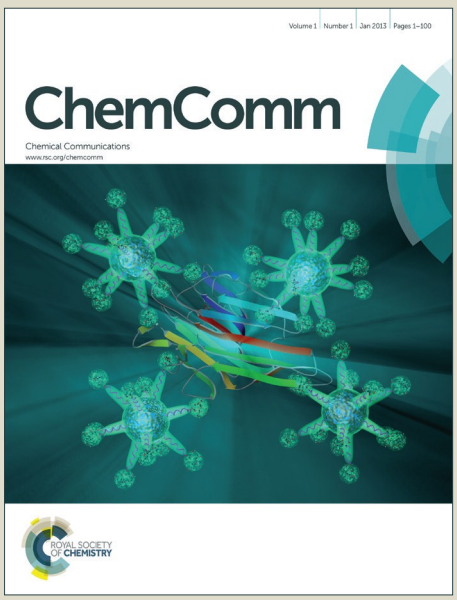

ROYAL SOCIETY OF CHEMISTRY

www.rsc.org/chemcomm

Cite this: DOI: 10.1039/c0xx00000x

www.rsc.org/xxxxxx

communication

Electrodeposited $Ni_XCo_{3-X}O_4$ nanostructured films as bifunctional oxygen electrocatalysts

Timothy N. Lambert,*[a] Julian A. Vigil,[a] Suzanne E. White,[a] Danae J. Davis,[a] Steven J. Limmer,[b] Patrick D. Burton,[c] Eric N. Coker,[d] Thomas E. Beechem,[e] Michael T. Brumbach[f]

Received (in XXX, XXX) Xth XXXXXXXXX 20XX, Accepted Xth XXXXXXXXX 20XX
DOI: 10.1039/b000000x

Nanostructured $Ni_xCo_{3-x}O_4$ films serve as effective electrocatalysts for both the oxygen reduction and oxygen evolution reactions in alkaline electrolyte.

The identification of a single cost-effective catalyst that can effectively perform both the oxygen reduction reaction (ORR)[1-4] and the oxygen evolution reaction (OER) could simplify design protocols[5] for re-chargeable metal-air batteries and regenerative fuel cells leading to the realization of efficient and practical devices.[6-8] Current commercial benchmark catalysts for oxygen electrochemistry are based on expensive and rare metals (e.g. Pt/C, Ru/C, Ir/C), alloys (e.g. Pt/Ru) or oxides (RuOx, IrO_x), ultimately preventing their widespread use. These catalysts are also effective at performing either the oxygen reduction reaction (ORR) (e.g. Pt/C), or the oxygen evolution reaction (OER) (e.g. Ir/C), but not both. Furthermore, these precious metal catalysts often suffer from instability and poor electrochemical selectivity. With this in mind, non-noble metal bi-functional catalysts are being developed. These include, but are not limited to the following: silver (Ag),[9] cobalt based perovskites ($La_{0.6}Ca_{0.4}CoO_3$,[10] $La_{0.6}Ca_{0.4}Co_{0.8}Ir_{0.2}O_3$[11]), spinels ($Co_3O_4$,[12] Cu^0/Co_3O_4,[13] $NiCo_2O_4$,[14,15] $CoMn_2O_4$[16,17]), cobalt carbonate hydroxides ($(Co(CO_3)_x(OH)_y)$,[18] manganese oxides (Mn_2O_3,[19] α-MnO_2[20]) also combined with metal organic frameworks [α-MnO_2/MIL-101(Cr)],[21] and various composites of carbon (C), graphene (G) and carbon nanotubes (CNTs) ($La_{0.5}Sr_{0.5}Co_{0.8}Fe_{0.2}O_3$/G[22], G/CNT,[23] Co_3O_4/G,[24] $MnCo_2O_4$/G,[25] $CoFe_2O_4$/G,[26] Co_3O_4/C[27]).

The *in situ* preparation of catalysts directly onto substrates without the need for additional (inactive) binders or conductive additives is one approach to increase catalyst efficacy and utility. Direct contact with the underlying substrate/current collector promotes mechanical adhesion and facile interfacial electron transfer between the current collector and the catalyst, while meso- and nano-structuring has the advantages of porosity (which promotes rapid ion diffusion) and high surface area (on which the reaction takes place).[28,29] In the present work, several nanostructured mesoporous Ni-doped cobalt-based spinel oxide films (e.g. $Ni_xCo_{3-x}O_4$ with ~ $0 \leq x < 1$) were prepared without the use of a template, directly onto nickel foil utilizing a two-step electrodeposition-thermal annealing process. We demonstrate that the amount of nickel (Ni, as ions) in the $Ni_xCo_{3-x}O_4$ films can be varied simply by changing the molar ratio of Co:Ni in the solution used for electrochemical deposition. The resulting Co_3O_4 and $Ni_xCo_{3-x}O_4$ films display excellent activity for the ORR and OER. While the inclusion of Ni leads to increased activity, the most active catalyst was found to be one with the least amount of Ni in the structure. The catalysts developed here have similar overall oxygen electrode activity to that of commercial benchmarks for both the ORR, (e.g. *vs.* 20% Pt/C) and the OER (e.g. *vs.* 20% Ir/C) when examined in alkaline electrolyte (0.1 M KOH), under a range of mass loadings. Additionally, the films also show superior electrochemical stability and selectivity for ORR in the presence of MeOH. Despite the advantages of potentially lower cost, environmental compatibility and overall availability, only a few reports exist to date on bifunctional $Ni_xCo_{3-x}O_4$ catalysts,[30] and most of these rely on conductive graphene[14] or carbon additives.[15,31] To the best of our knowledge this is the first report of ORR/OER bifunctional $Ni_xCo_{3-x}O_4$ catalysts prepared using a template-less electrodeposition approach.

The synthesis of Co_3O_4 and $Ni_xCo_{3-x}O_4$ films on nickel foil was achieved using an electrodeposition-thermal annealing methodology as described in the ESI.† Briefly, solutions of either $Co(NO_3)_2$ or a defined ratio of $Co(NO_3)_2$:$Ni(NO_3)_2$ in EtOH:H_2O (v:v 1:1) with aqueous $NaNO_3$ as the supporting electrolyte were used to deposit metal hydroxide films.[32,33] Mass deposition rates of 29.9 ± 1.13 μg cm^{-2} min^{-1} (for Co solution) and 29.0 ± 0.37 μg cm^{-2} min^{-1} (for Co and Ni solution at 1:0.5 molar ratio), were determined using a quartz crystal microbalance (QCM) and indicate that the rate of deposition is nearly identical for all

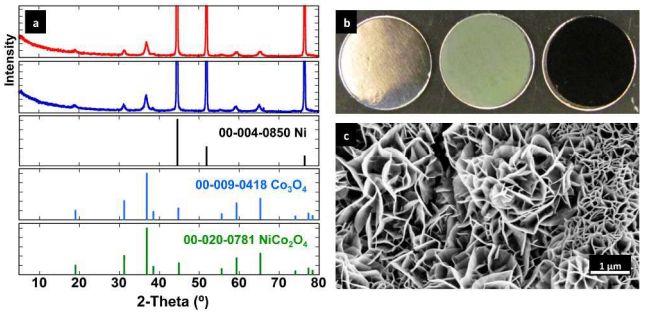

Fig. 1 a) XRD of Co_3O_4 (top, red) and $Ni_{0.6}Co_{2.4}O_4$ (bottom, blue); b) Image of (left to right) Ni foil, (as deposited) $Co_{1-z}Ni_z(OH)_{2-x}(NO_3)_x \bullet y(H_2O)$ and (thermally annealed) $Ni_{0.6}Co_{2.4}O_4$ on Ni; c) SEM of $Ni_{0.6}Co_{2.4}O_4$ film on Ni foil.

solutions, Fig. S1 (ESI†). Conversion of the resulting $Co_1(OH)_{2-x}(NO_3)_x \bullet y(H_2O)$ or $Co_{1-z}Ni_z(OH)_{2-x}(NO_3)_x \bullet y(H_2O)$ films to the spinel oxide (i.e. Co_3O_4 or $Ni_xCo_{3-x}O_4$) was readily achieved by thermal annealing at 300 °C in air, Fig. 1. Grazing angle X-ray diffraction (XRD) spectra shown in Fig. 1a and Fig. S2 (ESI†) confirms the formation of the spinel phase, indexed to Co_3O_4 or $NiCo_2O_4$; JCPDS file nos. 009-0418 or 020-0781, respectively. No other phases were detected. This conversion is also observed as a colour change in the film, from green to black, Fig. 1b. Scanning electron microscopy (SEM) micrographs shown in Fig. S3 (ESI†) and Fig. 1c demonstrate the nano-textured surface and meso-porous nature of the electrodeposited films, and that these features are retained upon heating. Thermal gravimetric analysis (TGA) was used to quantify the mass loss (~ 25%) upon conversion from the metal hydroxide to metal oxide during thermal annealing in order to determine the mass of spinel resulting on the film, Table S1 (ESI†).

Acid digestion of films after mechanical removal from the substrate, followed by elemental analysis with Inductively Coupled Plasma/Mass Spectrometry (ICP/MS), indicates the formation of $Ni_xCo_{3-x}O_4$ films with a partial stoichiometric substitution of Ni into the spinel structure. For example, the film prepared from the 1:0.5 Co:Ni solution ratio gave a resulting formula of $Ni_{0.6}Co_{2.4}O_4$ as opposed to the theoretical $NiCo_2O_4$, indicating only 59% of the theoretical Ni being incorporated. 59% partial incorporation was also observed for films with less (Co:Ni ratio = 1:0.25, yielding $Ni_{0.4}Co_{2.6}O_4$) or more (Co:Ni ratio = 1:1, yielding $Ni_{0.9}Co_{2.1}O_4$) Ni in the original solution, Table S2 (ESI†). These values are consistent with the nearly identical mass deposition rates across all Co:Ni ratios as observed from the QCM data in Fig, S1 (ESI†) and reasonable given the estimated solubility for Co^{2+} or Ni^{2+} in the electrolyte, Fig. S4 (ESI†).

Co_3O_4 and $Ni_xCo_{3-x}O_4$ films were then evaluated for their ability to act as catalysts for reversible oxygen electrochemistry, as determined from linear scanning voltammetry (LSV) methods.† Averaged data from Co_3O_4, $Ni_{0.6}Co_{2.4}O_4$, commercial benchmark standards [20% Pt/C (from E-tek™) and 20% Ir/C (from Premetek™) along with Ni foil background for the ORR are shown in Fig. 2a. The Co_3O_4 film demonstrates good catalytic activity for the ORR despite having no conductive carbon or binder, while the inclusion of Ni improves the performance of the $Ni_{0.6}Co_{2.4}O_4$ spinel film relative to Co_3O_4 for the ORR. Specifically, while the onsets of reduction for the two are nearly identical (0.88 V *vs.* RHE), the half-wave potential (and half-wave current density) [0.768 V (-3.29 mA cm^{-2})] and terminal current density (-6.57 mA cm^{-2}) for $Ni_{0.6}Co_{2.4}O_4$ is much improved over Co_3O_4 [0.692 V (-2.82 mA cm^{-2}) and -5.63 mA cm^{-2}], respectively. Comparison of ORR activity to commercial 20% Pt/C is also very favorable. While the 20% Pt/C film has a 0.072 V more positive onset, it exhibits a ~ 30% lower half-wave current density (-2.36 mA cm^{-2}) and steady state current density (-4.72 mA cm^{-2}) than the $Ni_{0.6}Co_{2.4}O_4$ spinel film. The $Ni_{0.6}Co_{2.4}O_4$ film's current density surpasses the 20% Pt/C at ~ 0.8 V *vs.* RHE. This half-wave potential region is important, as it is generally the potential range where maximum power can be extracted from a fuel cell.[2,34] Fig. 2a also demonstrates that 20% Pt/C is a better ORR catalyst than 20% Ir/C, as expected. A

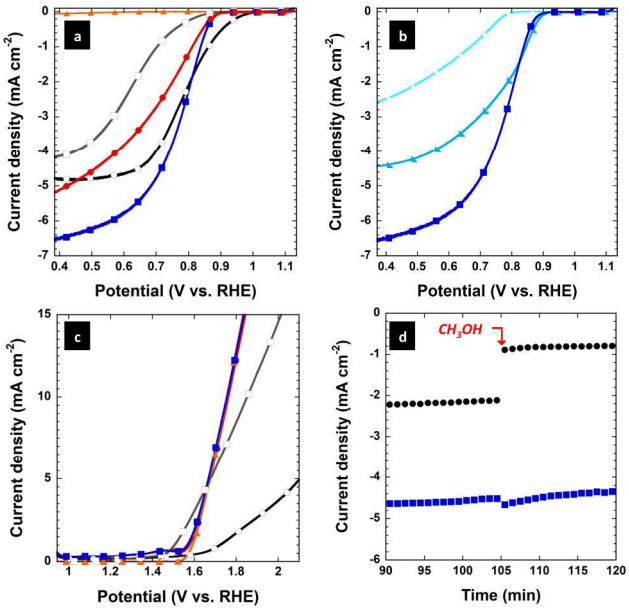

Fig. 2 ORR LSVs (@ 2500 rpm) for a) $Ni_{0.6}Co_{2.4}O_4$/Ni (blue, filled squares), 20% Pt/C (black, open circles), Co_3O_4/Ni (red, filled circles), 20% Ir/C (grey, open squares) and Ni foil (orange, filled triangles), b) $Ni_{0.6}Co_{2.4}O_4$ on Ni foil (blue, filled squares), 40% $Ni_{0.6}Co_{2.4}O_4$ powder/60% Vulcan XC-72 blend (medium blue, filled triangles) and $Ni_{0.6}Co_{2.4}O_4$ (light blue, open triangles); OER LSVs for c) $Ni_{0.6}Co_{2.4}O_4$/Ni (blue, filled squares), Co_3O_4/Ni (red, filled circles), Ni foil (orange, filled triangles), 20% Ir/C (grey, open squares) and 20% Pt/C (black, open circles); d) Chronoamperometric response for $Ni_{0.6}Co_{2.4}O_4$/Ni (blue, filled squares) *vs.* 20% Pt/C (black, filled circles) upon CH_3OH addition (2 wt. % final concentration) at 105 min.

comparison of the electrocatalytic properties of the $Ni_{0.6}Co_{2.4}O_4$ film on Ni foil, $Ni_{0.6}Co_{2.4}O_4$ powder removed from the Ni foil and $Ni_{0.6}Co_{2.4}O_4$ powder blended with Vulcan™ carbon and Nafion™ binder is provided in Fig. 2b. The data indicates that the high electrocatalytic activity for these films is a result of the continuous porous high surface area morphology of the spinel and its intimate contact with the conductive Ni foil substrate. For example, while the $Ni_{0.6}Co_{2.4}O_4$ powder electrocatalyst displays an *n* value (indicating the reaction order)[2-4] of 3.9, and low peroxide production, Fig. S5 and S6 (ESI†), it is considerably less effective than the porous $Ni_{0.6}Co_{2.4}O_4$/Ni film, even when blended with Vulcan carbon, Fig. 2b.

The OER data in Fig. 2c demonstrates that the Co_3O_4 and $Ni_{0.6}Co_{2.4}O_4$ films also outperform both 20% Pt/C and 20% Ir/C catalysts for the OER, as studied here. Ni foil is known to be an OER catalyst in alkaline media; however, the addition of the spinel film leads to improved onset values:† 1.58 V/RHE (Co_3O_4) and 1.57 V/RHE ($Ni_{0.6}Co_{2.4}O_4$) *vs.* 1.60 (for Ni foil). While 20% Ir/C displays an earlier onset value (1.51 V), the spinel films exhibit considerably lower voltages than 20% Ir/C (and 20% Pt/C) at 10 mA cm^{-2} with $Ni_{0.6}Co_{2.4}O_4$ (1.76 V) ~ Co_3O_4 (1.76 V) < 20% Ir/C (1.85 V) << 20% Pt/C (did not reach 10 mA cm^{-2} in our hands).† 10 mA cm^{-2} is chosen as an OER metric due to its relevance for solar fuels synthesis.[19,35] Fig 2c. also demonstrates that 20% Ir/C is a better OER catalyst than 20% Pt/C, as expected.

$Ni_xCo_{3-x}O_4$ films also displayed excellent electrocatalytic selectivity for ORR versus the electro-oxidation of methanol, unlike the 20% Pt/C catalyst. Fig. 2d shows chronoamperometric data for 20% Pt/C and $Ni_{0.6}Co_{2.4}O_4$ at their respective half-wave potentials. Upon the introduction of methanol at 105 min (resulting solution = 2 wt.% CH_3OH) the 20% Pt/C catalyst suffers a significant 46% decrease in current density, versus a modest 6% decrease (determined at 15 min after the addition) in current density for the $Ni_{0.6}Co_{2.4}O_4$ film.

A more positive voltage and better stability for the ORR was also observed with $Ni_{0.6}Co_{2.4}O_4$ as opposed to 20% Pt/C, under galvanostatic conditions of -3 mA/cm^2, Fig. 3a. -3 mA cm^{-2} was chosen as an approximate half wave current density for comparison purposes.[19] Similarly, a lower voltage with better OER stability was also observed for $Ni_{0.6}Co_{2.4}O_4$ ($\sim \leq 1.8$ V) as opposed to 20% Ir/C ($\sim \geq 1.9$ V), under galvanostatic conditions of 10 mA/cm^2, Fig. 3b. In fact, 20% Ir/C increases in voltage during the experiment while $Ni_{0.6}Co_{2.4}O_4$ decreases, likely due to surface inactivation and activation processes, respectively.

Given the observed increase in catalytic activity with Ni doping, the $Ni_xCo_{3-x}O_4$ films with more ($Ni_{0.9}Co_{2.1}O_4$) or less Ni doping ($Ni_{0.4}Co_{2.6}O_4$) than the $Ni_{0.6}Co_{2.4}O_4$ were also analyzed as electrocatalysts for ORR and OER, Fig. 3c and Fig. S7 (ESI†). Fig. 3c shows the surprising result that the most active film for ORR ($Ni_{0.4}Co_{2.6}O_4$) is the one with the least amount of Ni incorporation. Using the potential at -3 mA cm^{-2} as the ORR figure of merit,[19] we find the ORR activity follows the order of $Ni_{0.4}Co_{2.56}O_4 > Ni_{0.6}Co_{2.4}O_4 > Ni_{0.9}Co_{2.1}O_4 > Co_3O_4$.

Similar OER trends were found with $Ni_{0.4}Co_{2.56}O_4 > Ni_{0.6}Co_{2.4}O_4 > Ni_{0.85}Co_{2.15}O_4 > 1{:}0$ (Co_3O_4), using the metric of voltage at 10 mA cm^{-2};[19,35] however, the differences are small Fig S7 (ESI†). The difference between the OER and ORR metrics [Δ(OER-ORR)] was calculated in order to assess the overall oxygen electrocatalytic activity, where a smaller difference represents a more ideal reversible oxygen electrode.[19] In addition to outperforming the benchmark catalyst materials studied here, $Ni_{0.4}Co_{2.56}O_4$, with Δ(OER-ORR) = 0.96 V, is competitive with 20% Ir/C [Δ(OER-ORR) = 0.92 V] and 20% Pt/C [Δ(OER-ORR) = 1.16 V] values reported in the literature,[19] Table S3, (ESI†).

In order to evaluate the effect of the mass loading on catalyst performance, a series of films were prepared with different masses using the most ORR active Co:Ni ratio of 1:0.25. Specifically, $Ni_{0.4}Co_{2.6}O_4$ catalyst films of 5 μg (25.5 μg cm^{-2}), 12.5 μg (63.7 μg cm^{-2}) and 25 μg (127 μg cm^{-2}) were prepared and evaluated against 20% Pt/C (of equal masses). Fig. 3d shows that the $Ni_{0.4}Co_{2.6}O_4$ films are equal to or outperform 20% Pt/C for ORR across all mass loading examined. This data also indicates, as expected, that the most efficient films from a mass activity view are those that have the lowest mass.

Given that the electrocatalytic activity depends on both electronic and geometric factors, further considerations were undertaken in order to try to understand the effect of Ni in $Ni_xCo_{3-x}O_4$. Previous enhancements of electrocatalytic activity for $Ni_xCo_{3-x}O_4$ over that of Co_3O_4 have been assigned to an increase in specific surface area and roughness factor (geometric effect) and/or increase in conductivity (electronic effect). First, the electrochemically active surface area (ECSA) was estimated from the electrochemical double layer capacitance by measuring

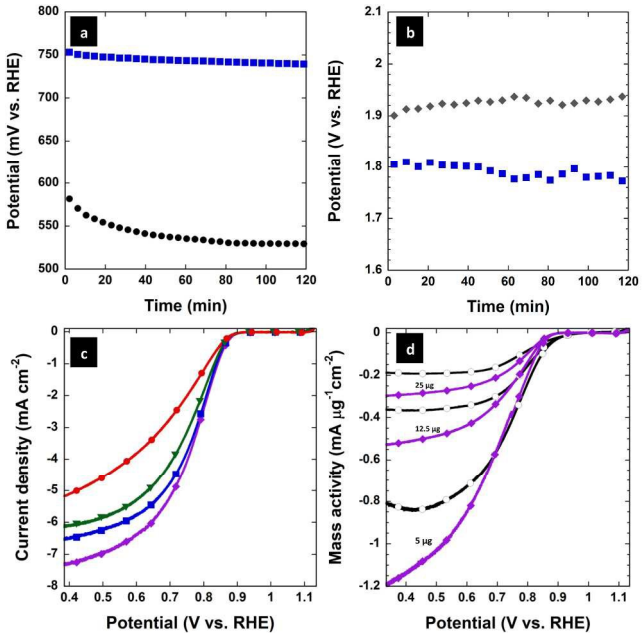

Fig. 3 Galvanostatic stability comparison between: $Ni_{0.6}Co_{2.4}O_4$/Ni (blue, filled squares) and a) 20% Pt/C (black, filled circles) for ORR (@ -3 mA cm^{-2}) and b) 20% Ir/C (grey, filled diamonds) for OER (@ 10 mA cm^{-2}); c) LSV (@2500 rpm) comparison for $Ni_{0.4}Co_{2.6}O_4$/Ni (purple, filled squares), $Ni_{0.6}Co_{2.4}O_4$/Ni (blue, filed squares), $Ni_{0.9}Co_{2.1}O_4$/Ni (green, filled triangles) and Co_3O_4 (red, filled circles); d) Mass activity comparison of $Ni_{0.4}Co_{2.6}O_4$/Ni (purple, filled squares) *vs.* 20% Pt/C (black, filled circles) at 5, 12.5 and 25 μg total catalysts

the non-Faradiac capactive current due to double layer charging from scan-rate dependent cyclic voltammograms,[35] Fig. S8 (ESI†). The data (using a oxide capacitance value of 40 μF cm^{-2})[35] suggests that increasing Ni content leads to a higher *relative* electrochemical surface area: with Co_3O_4 (42.6 ± 1.7 cm^2) < $Ni_{0.4}Co_{2.6}O_4$ (69.8 ± 7.0 cm^2) ~ < $Ni_{0.6}Co_{2.4}O_4$ (76.2 ± 6.6 cm^2) ~ < $Ni_{0.9}Co_{2.1}O_4$ (85.4 ± 8.1 cm^2). Brunauer-Emmett-Teller (BET) surface analysis on powders, after removal from the Ni foil, indicates Ni inclusion increases surface area with: Co_3O_4 (88.7 m^2 g^{-1}) < $Ni_{0.4}Co_{2.6}O_4$ (99.8 m^2 g^{-1}) ~ $Ni_{0.6}Co_{2.4}O_4$ (94.2 m^2 g^{-1}) ~ $Ni_{0.9}Co_{2.1}O_4$ (101.4 m^2 g^{-1}). The high BET surface areas obtained are comparable to those of recently reported nanowire arrays[36] and three-dimensional hierarchical structures[7] of $Ni_xCo_{3-x}O_4$. Increasing Ni in $Ni_xCo_{3-x}O_4$ has been reported to lead to an increase in surface area for spinels, with maxima reported for ~ $Ni_{0.6}Co_{2.4}O_4$[37] and $Ni_1Co_2O_4$.[7] The differences may be attributed to different methods of preparation.

Scherrer XRD analysis and Raman spectroscopy shown in Fig. S9 and S10 (ESI†), respectively, also suggest that increasing Ni content in the $Ni_xCo_{3-x}O_4$ films results in a smaller crystallite size. Combined TGA/MS data presented in Fig. S11 (ESI†) also shows a larger loss of O_2 upon heating to 650 °C for higher values of *x* in $Ni_xCo_{3-x}O_4$. These features, which are consistent with the presence of a higher number of crystalline edge defect sites for higher *x* values in $Ni_xCo_{3-x}O_4$, could be expected to correlate with improved catalytic activity,[4] unlike the trend observed here. However, the larger crystallite size of $Ni_{0.4}Co_{2.6}O_4$ may be resulting in a more conductive spinel. It seems that the penalty induced by the Ni as it concerns conductivity may be larger than

the "gain" obtained via enhanced (electrochemical) surface area.

Conductivity studies on a series of spinel $Ni_xCo_{3-x}O_4$ ($0 \leq x \leq 1$) powders,[38] prepared from the respective nitrates at similar temperatures (300-350 °C), shows that the activation energy for conduction decreases with x and disappears almost completely between $x = 0.5$ and 0.6, near the transition from semi-conductor to semi-metallic nature of the oxide. The hypothesis that $Ni_{0.4}Co_{2.6}O_4$ is the most conductive sample here is supported by the fact that $Ni_{0.4}Co_{2.6}O_4$ had the lowest charge transfer resistance value of 0.44 kΩ: e.g. versus $Ni_{0.6}Co_{2.4}O_4$ (0.52 kΩ) and Co_3O_4 (0.62 kΩ). Subtle changes in metal ion site occupation and valence with changes in x in the $Ni_xCo_{3-x}O_4$ films are known to affect the conductivity of the spinel oxide.[37,39] Unfortunately, XPS analysis of these materials, as shown in Fig. S12 (ESI†), could not discern significant differences in valence of Ni in these films. An alternative possibility could be the presence of small discrete NiO crystallite domains at higher values of x, which negatively effects performance and/or conductivity. While Raman spectroscopy data provided in Fig. S10 (ESI†) was found to corroborate the spinel phase for all $Ni_xCo_{3-x}O_4$ films, the presence of NiO cannot be ruled out due to spectral overlap with the E_g and F_{2g} Raman peaks of $Ni_xCo_{3-x}O_4$ spinels.

In summary, $Ni_xCo_{3-x}O_4$ films prepared using a two-step electrodeposition-thermal annealing process on Ni foil, are promising bifunctional catalysts for use as reversible oxygen electrodes. This is attributed to their intimate contact with the underlying Ni substrate, high surface area, mesoporous structure and improved conductivity over Co_3O_4. Given the excellent electrocatalytic properties for oxygen electrochemistry with $Ni_xCo_{3-x}O_4$ films, further studies are warranted and will be reported in due course.

This work was supported by Sandia National Laboratories: Sandia is a multi-program laboratory operated by Sandia Corporation, a Lockheed Martin Company, for the United States Department of Energy's National Nuclear Security Administration under Contract DE-AC04-94AL85000. Ms. Bonnie McKenzie and Dr. Mark Rodriguez are thanked for technical assistance.

Notes and references

*Sandia National Laboratories, Albuquerque, New Mexico, 87185, USA, *Fax: 505 844 7786; Tel: 505 284 6967; E-mail: tnlambe@sandia.gov. Departments of: [a]Materials, Devices & Energy Technologies, [b]Physics Based Microsystems, [c]Chemical and Biological Systems, [d]Advanced Materials Laboratory, [e]Nanoscale Sciences, [f]Materials Characterization and Performance.* *† Unless stated, experiments were conducted with 25 μg (127 μg/cm²) catalyst loadings; OER performed on Ni/Ti/Au foil confirms the OER activity is due to the spinel; Pt/C and Ir/C were newly purchased. Attempts to activate the catalysts in reducing atmospheres failed to increase their activity. For comparison to representative literature Pt/C and Ir/C values refer to Table S3 in the ESI. Electronic Supplementary Information (ESI) available: [Additional Figures and Experimental Data as noted in the text]. See DOI: 10.1039/b000000x/*

1. T. N. Lambert, D. J. Davis, S. J. Limmer, M. R. Hibbs and J. M. Lavin, *Chem. Commun.,* 2011, **47**, 9597-9599.
2. T. N. Lambert, D. J. Davis, W. Lu, S. J. Limmer, P. G. Kotula, A. Thuli, M. Hungate, G. Ruan, Z. Jin and J. M. Tour, *Chem. Commun.*, 2012, **48**, 7931-7933.
3. D. J. Davis, A.-R. O. Raji, T. N. Lambert, J. A. Vigil, L. Li, K. Nan and J. M. Tour, *Electroanal.*, 2014, **26**, 164-170.
4. D. J. Davis, T. N. Lambert, J. A. Vigil, M. A. Rodriguez, M. T. Brumbach, E. N. Coker and S. J. Limmer, *J. Phys. Chem. C*, 2014, **118**, 17342-17350.
5. Y. Li, M. Gong, Y. Liang, J. Feng, J.-E. Kim, H. Wang, G. Hong, B. Zhang and H. Dai, *Nat. Commun.*, 2013, **4**, 1805.
6. L. Jörissen, *J. Power Sources*, 2006, **155**, 23-32.
7. P. Manivasakan, P. Ramasamy and J. Kim, *Nanoscale*, 2014, **6**, 9665-9672.
8. J. Zhang, P. Li, Z. Wang, J. Qiao, D. Rooney, W. Sun and K. Sun, *J. Mater. Chem. A*, 2015, **3**, 1504-1510.
9. N. Sasikala, K. Ramya and K. S. Dhathathreyan, *Energ. Convers. Manage.*, 2014, **77**, 545-549.
10. S. Zhuang, K. Huang, C. Huang, H. Huang, S. Liu and M. Fan, *J Power Sources*, 2011, **196**, 4019-4025.
11. Y.-M. Chang, P.-W. Wu, C.-Y. Wu and Y.-C. Hsieh, *Journal of Power Sources*, 2009, **189**, 1003-1007.
12. D. U. Lee, J. Scott, H. W. Park, S. Abureden, J.-Y. Choi and Z. Chen, *Electrochem. Commun.*, 2014, **43**, 109-112.
13. W. Yang, J. Salim, C. Ma, Z. Ma, C. Sun, J. Li, L. Chen and Y. Kim, *Electrochem. Commun.,* 2013, **28**, 13-16.
14. D. U. Lee, B. J. Kim and Z. Chen, *Journal of Materials Chemistry A*, 2013, **1**, 4754-4762.
15. M. Prabu, K. Ketpang and S. Shanmugam, *Nanoscale*, 2014, **6**, 3173-3181.
16. L. Wang, X. Zhao, Y. Lu, M. Xu, D. Zhang, R. S. Ruoff, K. J. Stevenson and J. B. Goodenough, *J. Electrochem. Soc.*, 2011, **158**, A1379-A1382.
17. F. Cheng, J. Shen, B. Peng, Y. Pan, Z. Tao and J. Chen, *Nature Chem.*, 2011, **3**, 79-84.
18. Y. Wang, W. Ding, S. Chen, Y. Nie, K. Xiong and Z. Wei, *Chem. Commun.*, 2014, **50**, 15529-15532.
19. Y. Gorlin and T. F. Jaramillo, *J. Am. Chem. Soc.,* 2010, **132**, 13612-13614.
20. Y. Meng, W. Song, H. Huang, Z. Ren, S.-Y. Chen and S. L. Suib, *J. Am. Chem. Soc.*, 2014, **136**, 11452-11464.
21. F. Yin, G. Li and H. Wang, *Catal. Commun.*, 2014, **54**, 17-21.
22. H. W. Park, D. U. Lee, P. Zamani, M. H. Seo, L. F. Zazar and Z. Chen, *Nano Energy*, 2014, **10**, 192-200.
23. H. W. Park, D. U. Lee, Y. Liu, J. Wu, L. F. Nazar and Z. Chen, *J. Electrochem. Soc.*, 2013, **160**, A2244-A2250.
24. Y. Liang, Y. Li, H. Wang and H. Dai, *J. Am. Chem. Soc.*, 2013, **135**, 2013-2036.
25. H. Wang, Y. Yang, Y. Liang, G. Zheng, Y. Li, Y. Cui and H. Dai, *Energ. Environ. Sci.*, 2012, **5**, 7931-7935.
26. W. Bian, Z. Yang, P. Strasser and R. Yang, *J. Power Sources*, 2014, **250**, 196-203.
27. T. Y. Ma, S. Dai, M. Jaroniec and S. Z. Qiao, *J. Am. Chem. Soc.*, 2014, **136**, 13925-13931.
28. S. Chabi, C. Peng, D. Hu and Y. Zhu, *Adv. Mater.*, 2014, **26**, 2440-2445.
29. X. Yu, Z. Sun, Z. Yan, B. Xiang, X. Liu and P. Du, *J. Mater. Chem. A*, 2014, **2**, 20823-20831.
30. C. Jin, F. Lu, X. Cao, Z. Yang and R. Yang, *J. Mater. Chem. A*, 2013, **1**, 12170-12177.
31. S. Chen and S.-Z. Qiao, *ACS Nano*, 2013, **7**, 10190-10196.
32. J.-S. Do and R.-F. Dai, *J. Power Sources*, 2009, **189**, 204-210.
33. E. B. Castro, S. G. Real and L. F. Pinheiro Dick, *Int. J. Hydrogen Energ.*, 2004, **29**, 255-261.
34. R. J. Stanis, T. N. Lambert and M. A. Yaklin, *Energ. Fuel.*, 2010, **24**, 3125-3129.
35. C. C. L. McCrory, S. Jung, J. C. Peters and T. F. Jaramillo, *J. Am. Chem. Soc.*, 2013, **135**, 16977-16987.
36. Y. Li, P. Hasin and Y. Wu, *Adv. Mater.*, 2010, **22**, 1926-1929.
37. L. A. De Faria, M. Prestat, J. F. Koenig, P. Chartier and S. Trasatti, *Electrochim. Acta*, 1998, **44**, 1481-1489.
38. N. K. Appandairajan and J. Gopalakrishnan, *P. Indian Acad. Sci. A*, 1978, **87**, 115-120.
39. C. F. Windisch, K. F. Ferris and G. J. Exarhos, *J. Vac. Sci. Technol. A*, 2001, **19**, 1647-1651.